Large-scale detection and characterization of interchromosomal rearrangements in normozoospermic bulls using massive genotype and phenotype data sets

Jeanlin Jourdain, Harmonie Barasc, Thomas Faraut, et al.

Genome Res. 2023 33: 957-971 originally published online July 6, 2023
Access the most recent version at doi:10.1101/gr.277787.123

Method

Large-scale detection and characterization of interchromosomal rearrangements in normozoospermic bulls using massive genotype and phenotype data sets

Jeanlin Jourdain,[1,2] Harmonie Barasc,[3] Thomas Faraut,[3] Anne Calgaro,[3] Nathalie Bonnet,[3] Camille Marcuzzo,[4] Amandine Suin,[4] Anne Barbat,[2] Chris Hozé,[1,2] Florian Besnard,[2,5] Sébastien Taussat,[1,2] Cécile Grohs,[2] Claire Kuchly,[4] Carole Iampietro,[4] Cécile Donnadieu,[4] Alain Pinton,[3] Didier Boichard,[2] and Aurélien Capitan[1,2]

[1]*Eliance, 75012 Paris, France;* [2]*Université Paris-Saclay, INRAE, AgroParisTech, GABI, G2B, 78350 Jouy-en-Josas, France;* [3]*GenPhySE, Université de Toulouse, INRAE, ENVT, 31320 Castanet-Tolosan, France;* [4]*INRAE, US 1426, GeT-PlaGe, Genotoul, France Génomique, Université Fédérale de Toulouse, 31320 Castanet-Tolosan, France;* [5]*Idele, 75012 Paris, France*

In this paper, we developed a highly sensitive approach to detect interchromosomal rearrangements in cattle by searching for abnormal linkage disequilibrium patterns between markers located on different chromosomes in large paternal half-sib families genotyped as part of routine genomic evaluations. We screened 5571 families of artificial insemination sires from 15 breeds and revealed 13 putative interchromosomal rearrangements, 12 of which were validated by cytogenetic analysis and long-read sequencing. These consisted of one Robertsonian fusion, 10 reciprocal translocations, and the first case of insertional translocation reported in cattle. Taking advantage of the wealth of data available in cattle, we performed a series of complementary analyses to define the exact nature of these rearrangements, investigate their origins, and search for factors that may have favored their occurrence. We also evaluated the risks to the livestock industry and showed significant negative effects on several traits in the sires and in their balanced or aneuploid progeny compared with wild-type controls. Thus, we present the most comprehensive and thorough screen for interchromosomal rearrangements compatible with normal spermatogenesis in livestock species. This approach is readily applicable to any population that benefits from large genotype data sets, and will have direct applications in animal breeding. Finally, it also offers interesting prospects for basic research by allowing the detection of smaller and rarer types of chromosomal rearrangements than GTG banding, which are interesting models for studying gene regulation and the organization of genome structure.

[Supplemental material is available for this article.]

Interchromosomal rearrangements (IRs) are a variable group of cytogenetic abnormalities characterized by the transfer of genetic material between two nonhomologous chromosomes. These types of mutations can occur at different stages of cell life (Weckselblatt and Rudd 2015). Robertsonian fusions are known to occur mostly during mitosis (Matveevsky et al. 2020), whereas complex rearrangements would be the result of defective meiosis (Burssed et al. 2022). Simple centromeric fusions are generally better tolerated than more complex structural variations, the latter being a common cause of reproductive problems and other pathogenic effects owing to meiotic defects and abnormal gene dosage or regulation (Popescu 1989; Scherer et al. 2007; Poot and Haaf 2015). To illustrate this fact, in humans, cytogenetic abnormalities are detected in ∼0.5% of newborns (Forabosco et al. 2009; Vasilevska et al. 2013), but their frequency increases to 5%–15% in infertile couples (Gekas et al. 2001; Clementini et al. 2005; Poornima et al. 2020), ∼25% in miscarriages and stillbirths, and up to 50%–60% in first-trimester miscarriages (Shaffer and Lupski 2000; Yatsenko and Rajkovic 2019).

Despite their potential impact on productivity, animal welfare, and economics, chromosomal aberrations in livestock species have received much less attention than in humans. In cattle, for example, a recent literature review counted only 81 IRs (Iannuzzi et al. 2021), whereas hundreds of thousands would be expected given a global bovine population of 1.5 billion heads at the end of 2022 (https://www.fao.org/faostat/en/#data/QCL, last accessed October 27, 2022) and an estimated prevalence of at least 0.14% for reciprocal translocations alone (De Lorenzi et al. 2012). Several reasons may explain this situation. First of all, because cattle breeds are characterized by high inbreeding, the attention of clinical geneticists has been focused primarily on recessive defects over the past decades at the expense of other pathologies (Bourneuf et al. 2017). Moreover, there is no systematic cytogenetic analysis of reproducers, except in a few breeds segregating for an

Corresponding authors: jeanlin.jourdain@inrae.fr, aurelien.capitan@inrae.fr
Article published online before print. Article, supplemental material, and publication date are at https://www.genome.org/cgi/doi/10.1101/gr.277787.123.

ancestral Robertsonian (Rob(1;29)) translocation, which is easily identifiable without the use of GTG banding (Ducos et al. 2000a). This means that other chromosomal aberrations, such as reciprocal translocations, may be missed. In addition, certain breeding practices have acted as a filter to limit the prevalence of IR. Indeed, in selected populations, most of the gene pool is transmitted to the next generation through artificial insemination (AI) with semen from elite sires that have been declared normozoospermic after drastic control of sperm concentration, morphology, and motility (Kastelic and Thundathil 2008). Furthermore, these sires were historically subject to progeny testing in order to estimate their genetic merit. They were made to produce about 100 offspring whose performance, including female fertility, was evaluated for various traits before deciding if it was worth to inseminate tens to hundreds of thousands of females with their semen. At this step, the reproductive careers of males with low conception rates or repeated instances of congenital malformations, presumably owing to genetic defects, ended prematurely and their progeny excluded from the breeding programs.

From 2010, the implementation of genomic evaluation in livestock production, which consists in predicting the genetic value of each animal based on its genotype at thousands of genetic markers, has opened new perspectives. This technological revolution has led to the wide dissemination of semen from elite sires without prior progeny testing and, above all, to the accumulation of large data sets of SNP array genotypes, whole-genome sequences, and phenotypes that can be used to address a wide variety of scientific questions (Bourneuf et al. 2017; Zhao et al. 2022; Besnard et al. 2023).

In this article, we propose a population-wide method to detect IR carriers among 5571 normozoospermic bulls by leveraging the routine genotyping of their offspring for genomic evaluation and exploiting the assumed absence of linkage disequilibrium (LD) between markers from different chromosomes. In addition, we perform cytogenetic validation, long-read sequencing, and a series of complementary analyses to define the exact nature of the rearrangements identified, investigate their origins, and describe their clinical consequences.

Altogether, we present the most comprehensive and thorough screen for IRs compatible with normal spermatogenesis in livestock species.

Results

Estimation of LD significance thresholds by simulation

As a first step, we conducted a series of simulations using progeny genotypes of 100 bulls considered free of chromosomal abnormalities in order to determine the significance threshold ($P \leq 0.001$) of LD between markers from different chromosomes according to the size of the half-sib families (see Methods) (Fig. 1A). Obviously, these thresholds were higher when the number of offspring was lower and the minimum size of the sire families was set to more than 30 half-siblings.

Large-scale screening for IRs

In the next step, we analyzed 5571 paternal half-sib families from 15 different breeds and found significant LD patterns for 13 of them (2.33‰) (Fig. 1; Supplemental Figs. S1A–S13A). They consisted of nine Holstein, two Charolais, one Normande, and one Abondance pedigrees accounting for 1.56‰–7.57‰ of the bulls tested within their breeds. Overall, there was no significant difference in the proportions of putative IR carriers between the breeds studied.

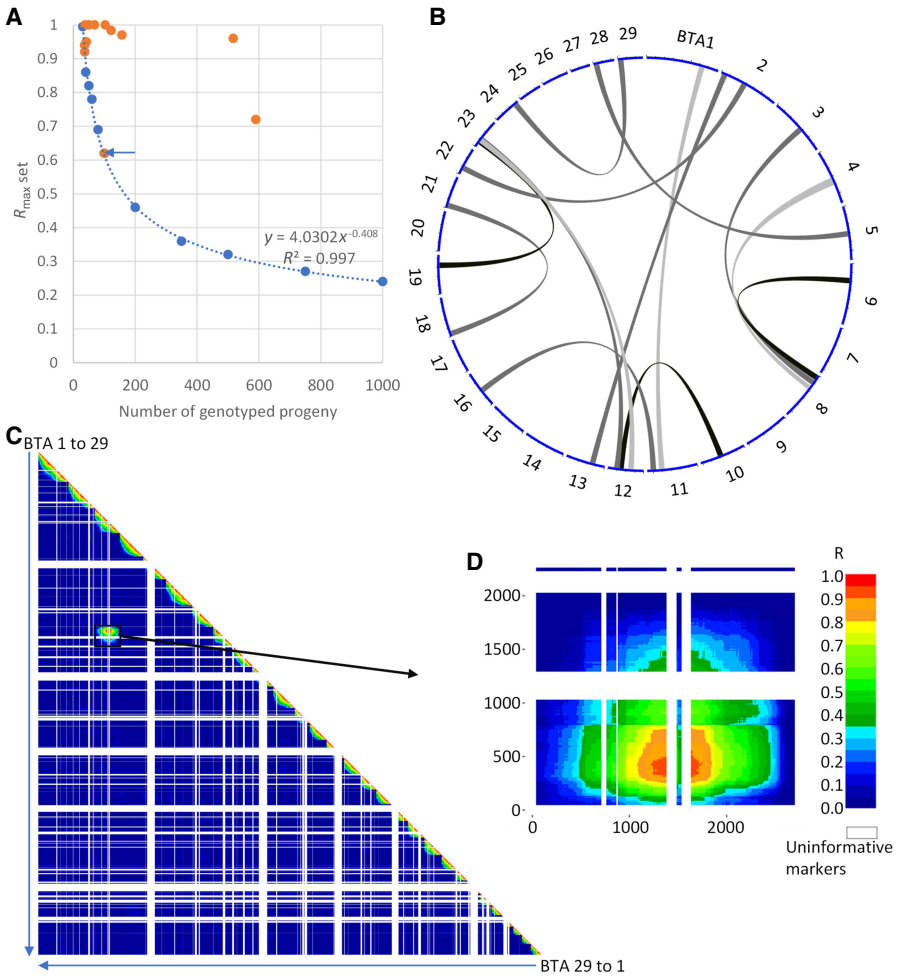

Figure 1. A novel approach to detect interchromosomal rearrangements (IRs) using SNP array genotypes in large half-sib families. (*A*) Regression curve of linkage disequilibrium (LD) significance thresholds ($P = 0.001$) obtained from series of 10,000 simulations. Blue dots indicate the results of simulations with 10 progeny group sizes ranging from 30 to 1000. Orange dots point to the maximal significant LD observed for 13 paternal half-sib families. (*B*) Circos plot (Yu et al. 2018; yimingyu.shinyapps.io/shinycircos/) representing the 13 rearrangements found. (*C*) Whole-genome LD map for a bull assumed to have an IR between BTA3 and BTA8. (*D*) Detail of the LD map between markers from these two chromosomes.

All rearrangements detected were unique in terms of the chromosomes and regions involved. Several chromosomes were overrepresented, with three occurrences for Chromosomes BTA12 and BTA23 (including two putative t(12;23) rearrangements) and two for BTA2, BTA8, and BTA11 (Fig. 1B). However, observing two or three times the same chromosome and even two times the same chromosome association out of 13 IRs was not unexpected by chance based on 100,000 series of random sampling with replacement ($P > 0.05$). In 11 cases, the maximum LD (R^2) was >0.9, whereas it only reached 0.72 and 0.61 for the bulls Nt and Ra, respectively (Fig. 1A).

Cytogenetic confirmation

For verification, we conducted cytogenetic analyses either directly on the sires, when they were still alive (applicable for one bull), or on a selection of their progeny representing each of the genotype combinations observed around putative chromosomal fusion points (sons and daughters for 10 bulls, granddaughters for two bulls). Analysis of blood lymphocytes in metaphase confirmed 12 of the 13 suspected rearrangements (Fig. 2B; Supplemental Figs. S1B–S13B, S1C–S13C, S1D–S13D). Thus, the validated prevalence of IR in our cohort of 5571 normozoospermic AI bulls was 2.15‰.

No karyotypic abnormality was observed among four daughters of the 13th bull, Ra, whereas the size of the segments putatively involved in the rearrangement exceeded the resolution limit of GTG banding (5–10 Mb). Note that this bull had the lowest significant LD value of the 13 putative IRs carriers (point with blue arrow in Fig. 1A). For two validated rearrangements, complementary fluorescence in situ hybridization (FISH) analyses were performed to increase the resolution. In one bull (Nt), a small segment of BTA4 inserted in BTA8 was barely visible. Using two probes targeting this BTA4 segment and the centromere of BTA8, we further confirmed the existence of this rearrangement and documented the presence of live monosomic and trisomic animals among its progeny (Fig. 2A; Supplemental Fig. S7J). For another bull (Ou), we suspected a reciprocal translocation between BTA24 and BTA29 and a loss of the derivative Chromosome 29. Marking the centromeres of all chromosomes confirmed our assumption (Supplemental Fig. S10J).

At the end of the cytogenetic analysis, we confirmed 12 IRs, consisting of one Robertsonian translocation, one insertional translocation, and 10 reciprocal translocations, including one with derivative loss. By analyzing the location of the breakpoints in more detail, we found that they were more frequently located in the third-quarter of the chromosomes than expected by chance ($P = 0.04$; chi-square) (Fig. 2C).

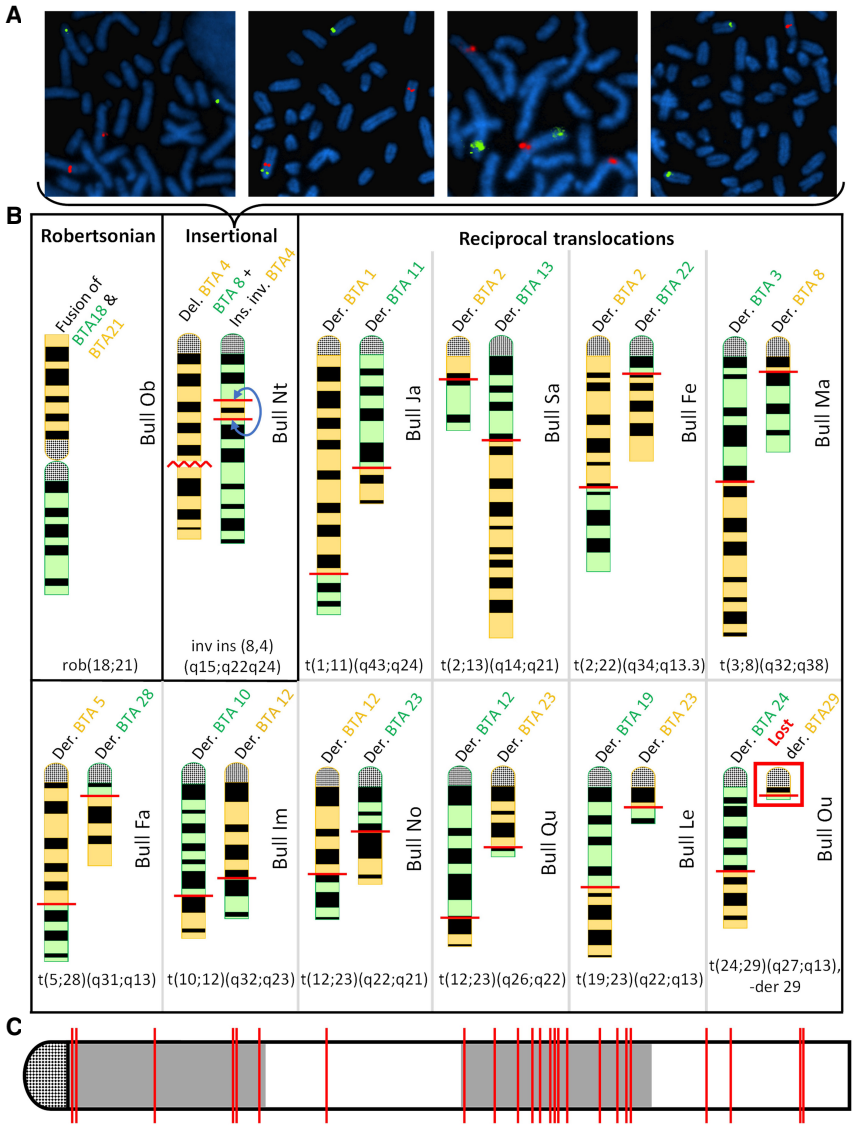

Figure 2. Validation of 12 IRs by cytogenetic analyses. (*A*) FISH mapping on cultured fibroblasts from four daughters of Nt with BAC clones located in the translocated segment from BTA4 (labeled in red) and in the centromeric region of BTA8 (labeled in green). From *left* to *right*, these animals show a normal karyotype, a balanced rearrangement, a partial BTA4 trisomy, and a partial BTA4 monosomy. (*B*) Schematic representation of the rearranged chromosomes based on GTG-banding karyotypes. Chromosomes with a loss or gain of material are shown in yellow and green, respectively. The schematics of the original chromosomes are available in Supplemental Figures S1D–S13D. (*C*) Location of the breakpoints on a theoretical chromosome. Coordinates are expressed as a percentage of chromosome length. Note the presence of 13 out of 24 breakpoints in the third quarter, whereas only six would be expected by chance.

Determining the origin and possible causes of rearrangement events

We then sought to determine in which animal and at what stage of development these mutations occurred. To achieve this goal, we set up haplotype tests to trace the segments involved in the rearrangements through generations, taking into account various

Table 1. Origins of interchromosomal rearrangements (IRs)

Bull	Rearrangement	Breed	Generation[a] (first mutant)	Cause
Ob	Rob(18;21)	Abondance	Third (maternal granddam)	Fusion between chromosomes in the zygote
Nt	inv ins(8;4)	Holstein	First	Abnormal male meiosis
Ja	t(1;11)	Normande	Second (dam)	
Sa	t(2;13)	Holstein	First	
Fe	t(2;22)	Holstein	First	
Ma	t(3;8)	Holstein	First	
Fa	t(5;28)	Holstein	First	
Im	t(10;12)	Holstein	First	
No	t(12−;23+)	Charolais	First	
Qu	t(12+;23−)	Holstein	First	
Le	t(19;23)	Charolais	First	
Ou	t(24;29),-der29	Holstein	First	Abnormal female meiosis

[a]Generation of mutants to which the detected bulls belong. For details on investigations, see Supplemental Figures S1F–S13F.

sources of information such as the parental origin of these segments, the co-occurrence (or not) of the two segments in the same ancestor, and the results of our initial screen for these ancestors. Indeed, the sires and maternal grandsires of the 12 IR carriers and, in some cases, more distant male ancestors were included in this analysis and were predicted to have normal karyotypes (for further details of the available data and the investigations performed within each pedigree, see Supplemental Figs. S1F–S13F). We determined that the Robertsonian translocation was probably the result of a chromosomal fusion at the zygote stage in the maternal granddam of the sire Ob. Ou's reciprocal translocation occurred during female meiosis, whereas the nine other reciprocal translocations and the insertional translocation were the result of abnormal male meiosis (Table 1; Supplemental Figs. S1F–S13F). Nine of the carriers of reciprocal translocations belonged to the first generation of mutants, whereas the last one was a second-generation mutant that inherited the two rearranged chromosomes from its carrier dam. Finally, it is worth noting that two carriers of distinct reciprocal translocations resulting from abnormal paternal meiosis (t(5;28) in Fa and t(2;22) in Fe) shared the same sire, which was tested as wild type along with 46 other of its sons in our initial screen. With a prevalence of 41.67‰ (2/48) of IR in its progeny versus 2.15‰ in the total cohort, this elite AI sire was a clear outlier.

Given the high proportion of IR caused by abnormal male meiosis (n = 10/12) and the general trend to collect semen of ever younger bulls, we compared the age of the sires at the conception of their mutant progeny with the weighted mean age at the conception of their 118 wild-type progeny included in our initial screen. We found no significant difference (3.33 ± 2.14 yr vs. 3.42 ± 2.24 yr, respectively; Student's t-test P-value = 0.93), indicating that the age of the sire at conception was not a factor influencing the risk of producing IR-affected progeny.

Characterization of the pathological consequences of IRs

To gain insight into the pathological consequences of these cytogenetic abnormalities, we then mined the French national database containing information on various aspects of the life of cows (such as their date of birth, death, insemination, and calving). The bulls used for this analysis had more than 30 progeny with available genotypes and were therefore all tested for the presence of IR.

First, we calculated conception rates (i.e., the proportion of inseminations that resulted in the birth of a calf) for 2900 bulls of the Holstein, Normande, Charolaise, and Abondance breeds, including the 12 IR carriers (Fig. 3A). Carriers of reciprocal translocations

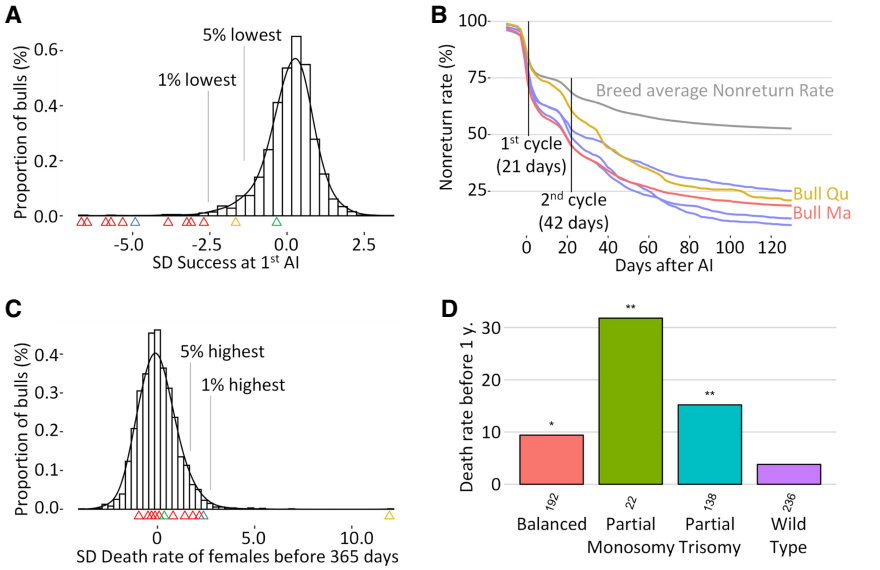

Figure 3. Analysis of conception rate, nonreturn rate (NRR), and juvenile mortality. (*A*) Conception rate of first artificial inseminations (1st AI) of 2900 bulls with nulliparous females, conventional semen, expressed as SD from the mean to allow comparison between bulls from different breeds. Arrowheads indicate carriers of the following IRs: red for reciprocal translocations, yellow for insertional translocation, gray for reciprocal with derivative loss, and green for Robertsonian translocation. (*B*) NRR for five affected Holstein bulls (i.e., the proportion of females that were not reinseminated after an insemination with the semen of the bull in question) and mean NRR of 2152 Holstein bulls. Two extreme bulls, Qu and Ma, are highlighted in red and yellow. (*C*) Mortality rates over the first year of life among the daughters of 2854 bulls considered, expressed as the SD from the mean of their respective breeds (same color code as in vignette *A*). (*D*) Distribution of mortality rates at 1 yr of age for Nt's progeny (*n below* bars). (*) Fisher comparison with wild-type group $P < 0.05$, (**) $P < 0.01$.

were all in the lowest percentile of their breed for this trait, and together, they explained 35% of the normozoospermic bulls affected by idiopathic subfertility (i.e., in the lowest 1% of their breed for conception rate).

A detailed analysis of the nonreturn rates (NRRs; i.e., the proportion of females probably pregnant at a given time after the insemination, given that they have no new AI) revealed different patterns of embryonic loss for these subfertile IR-affected bulls (Fig. 3B; Supplemental Figs. S1E–S11E). For example, the bull Ma showed an early drop in NRR compatible with a loss of aneuploid conceptuses at the beginning of embryogenesis, whereas the loss for Qu was more progressive and extended over a period covering organogenesis and beyond.

We also calculated mortality rates between birth and 1 yr of age in the female offspring of 2854 bulls, including the same 12 IR carriers (Fig. 3C), and found that four IR carriers were in the worst 5% of their breed. The bull Nt, carrying a large insertional translocation, was the worst sire of all breeds, with as much as 44% of daughters dying of natural causes before the age of 1 yr. Following the observation of live aneuploid progeny for this bull during cytogenetic analyses (see FISH in Fig. 2A), we estimated the proportion of normal and abnormal karyotypes based on haplotype test in 588 of its descendants that had been genotyped for genomic evaluation. We found that 40% of them were wild type, 33% had a balanced karyotype like their sire, and only 23% and 4% showed partial BTA4 trisomy and monosomy, respectively. We also observed significantly higher mortality rates <1 yr of age in carriers of abnormal karyotypes than in wild-type daughters (Fig. 3D).

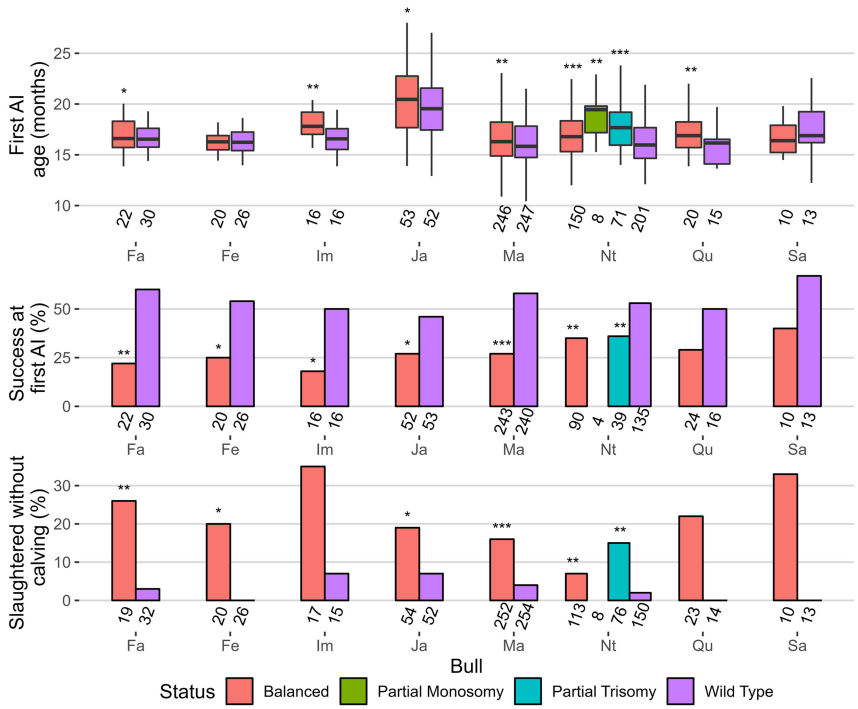

Figure 4. Comparison of the performance of daughters with normal and abnormal karyotypes among the progeny of nine IR-affected bulls. Cohort sizes are given *below* each bar. Significance levels refer to comparisons with wild type groups. Student's *t*-test for first AI, Fisher's test for the other traits): (*) $P<0.1$; (**) $P<0.05$; (***) $P<0.01$.

Finally, still based on haplotype tests, we analyzed the performance of the progeny of eight IR-affected dairy bulls that had sufficient data for three traits recorded in heifers (Fig. 4). For six of them, we observed a significant delay in age at first insemination, which is a proxy for growth, considering that dairy heifers are usually inseminated when they reach 60% of the expected adult weight. Field examination of the progeny of the bull Nt further confirmed this result (Supplemental Fig. S7K). Carriers of abnormal karyotypes also showed a significantly lower insemination success rate for six out of eight bulls studied. Consistent with the low performance observed for the previous two traits, we also observed a significant increase in the proportion of females slaughtered before starting a productive life among carriers of abnormal karyotypes versus half-sib controls for five bulls. Note that the progeny of bulls Ou and Ob were too young at the time of writing to reach significant numbers. We have not included Charolais phenotypes in this part because delaying AI is often a breeder's choice in this breed.

Long-read sequencing of seven IR carriers

To characterize the fusion points of the rearrangements, we sequenced the genomes of seven affected bulls at 32× unique molecular yield (UMY) coverage using Pacific Biosciences' (PacBio's) continuous long-read (CLR) technology (Fig. 5C,D; Supplemental Figs. S1G–S10G). These bulls were affected by an insertional translocation (Nt), a reciprocal translocation with derivative loss (Ou), and five different reciprocal translocations (Fe, Fa, Ja, Le, and Ma). In doing so, we were able to retrieve chimeric reads encompassing each of the fusion points, thus allowing determination of the coordinates of the segment forming the derivative chromosomes (Table 2) except for Fe (affected by a t(2;22)). For the latter, we observed a breakpoint on BTA2 around position 60,476,739 bp and chimeric reads containing up to 32 kb of BTSAT2 repeats on each side. We assumed that this material came from BTA22, but we were not able to confirm this hypothesis because of the highly repetitive nature of this component of the centromeres and because of the fact that centromeric regions are largely absent from the ARS-UCD1 assembly. We then investigated the exact nature of the fusion points and their possible consequences on the expression of neighboring genes. Information about breakpoint locations, neighboring candidate genes, and the possible consequences of their haploinsufficiency is presented in Tables 2 and 3. Annotated maps of chromosomal segments affected by the breakpoints are provided in panels H of Supplemental Figures S1–S10. For Ou, we confirmed the results of FISH experiments (Fig. 2B) supporting the absence of the derived Chromosome 29 and determined that it was partially monosomic for the last 3.9 Mb of BTA24 and the first 3.2 Mb of BTA29 (Fig. 5B; Supplemental Fig. S10I). The same bull presented an unexpected inversion of ~6 kb at the BTA24 breakpoint level. We also observed a heterozygous deletion of 1.9 Mb at the breakpoint on BTA3 in Ma (t(3;8); Fig. 5A). The regions deleted in these two bulls contained 29 and five genes, respectively, including, for Ou, several whose

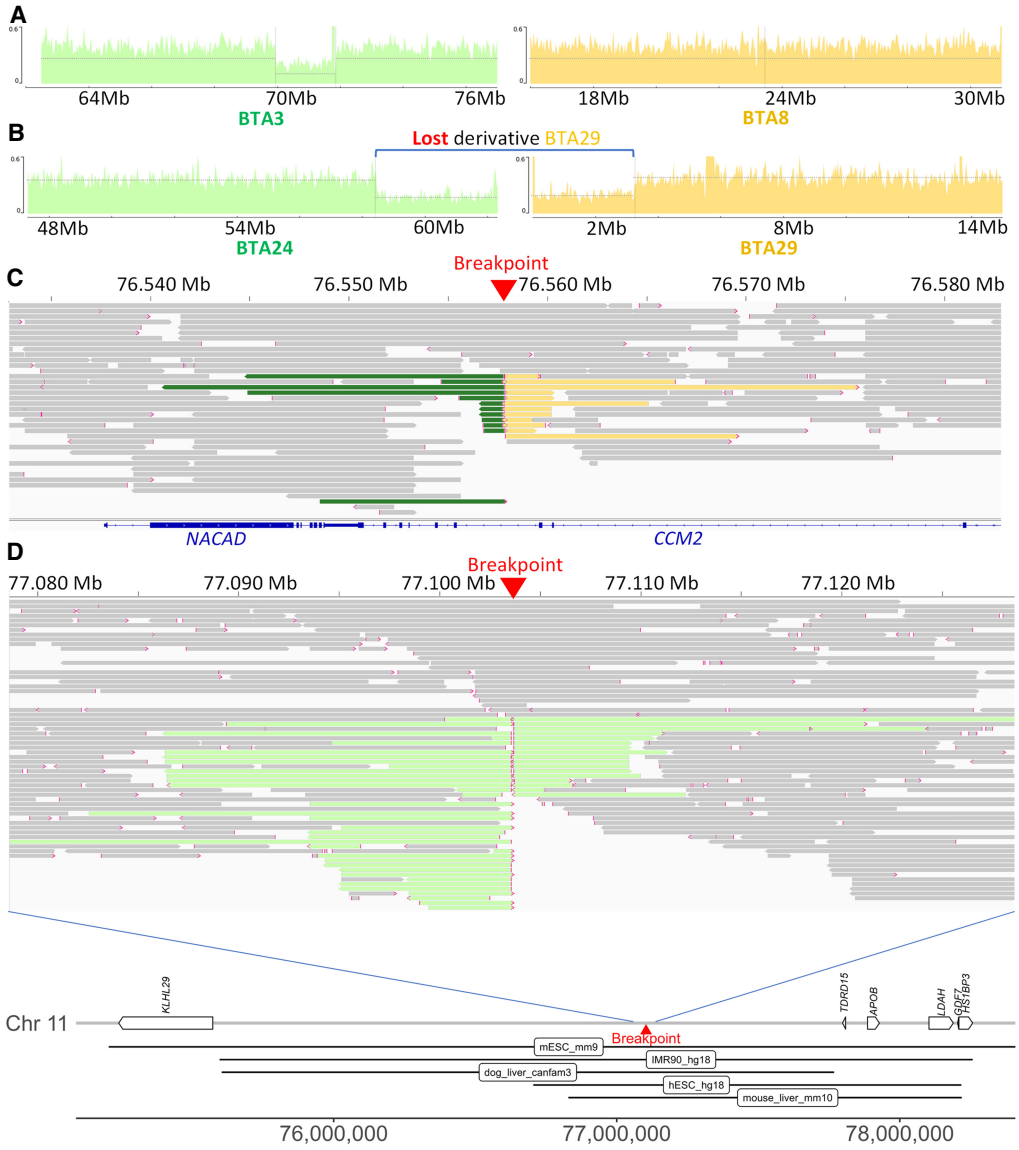

Figure 5. Contribution of PacBio CLR sequencing to the characterization of IR break points and fusion points. (*A*) Sequence coverage plots around the breakpoints of t(3;8) supporting a heterozygous deletion of ~2 Mb on BTA3 of bull Ma. (*B*) Sequence coverage plots around the breakpoints of t(24;29),-der29 supporting a loss of the derivative chromosome of bull Ou. For vignettes *A* and *B*, control alignments are provided in Supplemental Figures S6I and S10I. (*C*) Read alignment around the second breakpoint of inv ins(8,4) at 76.6 Mb on BTA4 (bull Nt). Split reads that also map to BTA8 and to BTA4 around position 65.9 Mb are colored in green and yellow, respectively. Note that the breakpoint resulted in the disruption of *CCM2*. (*D*, *top*) Read alignment around the breakpoint of t(1;11) on BTA11 with split read aligning to BTA1 colored in light green (bull Ja). (*D*, *bottom*) Details of the genes and putative TADs (according to Wang et al. 2018) located around the breakpoint of t(1;11) on BTA11.

haploinsufficiency has previously been implicated in various mouse and human pathologies (Table 3). Apart from these cases, the other breakpoints and fusion points consisted of deletions or insertions of only a few nucleotides. Three of them resulted in gene disruption, and all were predicted to affect a topologically associated domain (TAD) based on orthology comparison with human, mouse, and dog (Fig. 5E; Table 3; Supplemental Figs. S1H–S10H).

In addition, for each of the seven bulls, we observed that one breakpoint was located in a repeated element, whereas the second was not. These repeats were of different types (Supplemental Table S4) and even differed between the two paternal half-brothers Fa and Fe.

As a final attempt to identify potential genetic factors promoting IR, we sought to determine whether the breakpoints were located within recombination hotspots. For five IRs resulting from abnormal male meiosis with precise breakpoint coordinates, we analyzed the LD between the closest informative SNPs on either side of the breakpoint among the genotyped descendants of the sires that produced the mutant spermatozoid. This LD was then ranked in terms of percentiles compared with the LD between all informative SNPs separated by a similar distance along the same chromosome and along all other chromosomes. We did not observe any ranking <5% and therefore concluded that none of the breakpoints were located in recombination hotspots (see Supplemental Table S3).

Table 2. Information on the composition of the derivative chromosomes of seven IR carriers

Bull	IR	Coordinates (in base pairs) of the segments forming the derivative chromosomes
Fa	t(5;28)	der5: BTA5:start-74,392,483 + BTA28:2,572,392-end der28: BTA28:start-2,572,392 + BTA5:74,392,486-end
Fe	t(2;22)	*der2: BTA2:start-60,476,739 + BTA22:?* *der22: BTA22 ? + BTA2: 60,476,740-end*
Ja	t(1;11)	der1 BTA1:start-128,820,473 + BTA11:77,103,694-end der11: BTA11:start-77,103,581 + BTA1:128,820,484-end
Le	t(19;23)	der19: BTA19:start-56,469,717 + BTA23:9,681,308-end der23: BTA23:start-9,681,296 + BTA19:56,469,745-end
Ma	t(3;8)	der3: BTA3:start-69,934,844 + BTA8:23,449,822-end der8: BTA8:start-23,449,821 + BTA3:71,854,166-end
Nt	inv ins(8,4)	der4: BTA4:start-65,642,800 + BTA4:76,557,789-end der8: BTA8:start-37,638,721 + inv(BTA4:65,642,808-76,557,778) + BTA8:37,638,723-end
Ou	t(24;29) -der 29	der24: 24:start-58,418,700 + inv(24:58,418,700-58,424,275) + 29:3,257,559-end

Discussion

On the power of our approach

Analyzing 5571 paternal half-sib families with 31 or more genotyped progeny, we highlighted 13 putative IR ($P \leq 0.001$) using the approach developed in this study. Subsequent cytogenetic analyses revealed only one false positive, which is quite satisfactory, as five or six were expected given the sample size and the false-discovery rate chosen. Therefore, we estimated the prevalence of IR in our cohort of AI sires to be 2.15‰ (12/5571), which is similar to findings in normozoospermic males from other species. Indeed, 2.06‰ of 10,202 human sperm donors and 4.7‰ of 7700 AI boars were affected by IR according to Ravel et al. (2006) and Ducos et al. (2007), respectively.

Our strategy has led to significant advances in the detection of cytogenetic abnormalities in cattle, with the first report of an insertional translocation in this species (inv ins(8,4)(q15;q22q24)) and the identification of 10 new reciprocal translocations (rcp), whereas only 20 had been described previously (Iannuzzi et al. 2021). We also identified a new Robertsonian fusion (Rob (18;21)). These 12 events are unique. The proportions of the different types of IR highlighted in our study differ markedly from previous findings (0 inv ins, 20 rcp, and 61 Rob reviewed by Iannuzzi et al. 2021; $P = 1.3 \times 10^{-5}$ for Fisher's exact test for comparison of Rob vs. non-Rob translocations) but are consistent with the predictions of De Lorenzi et al. (2012), who estimated that reciprocal translocations would be at least five times more frequent than Robertsonian fusions in terms of de novo mutations events. This result reflects a major bias toward the detection of Robertsonian fusion in cattle, which is because of the lack of routine cytogenetic screening outside of a few breeds segregating for the Rob(1;29) translocation. Because Rob(1;29) and other submetacentric chromosomes formed by Robertsonian fusion are easily identifiable among the acrocentric bovine autosomes, they are tested by simple Giemsa staining, which hinders the detection of other types of translocations if they do not cause major changes in long arm length. To detect them, more accurate methods are needed, such as the GTG banding used for validation purpose in this study. However, even these are not infallible. In our experience, the insertion of an 11-Mb segment from BTA4 into BTA8 (inv ins(8,4)) would have been missed in a blind test because of its size, which is close to the resolution limit of banding (~5–10 Mb). The approximate knowledge of the breakpoint provided by LD analysis and FISH was instrumental in showing the existence of this novel type of IR in cattle.

As designed, our strategy is sensitive enough to detect translocations involving segments of only a few kilobases (containing at least one marker), with at least 30 genotyped progeny under the best conditions. As explained in the Methods, we recorded for each family the highest LD value between markers from different chromosomes (absolute correlation between alleles, also called R_{max}), and if the latter was significant ($P < 0.001$), we applied a filter to avoid spurious and punctual LD. We kept R_{max} only if the two markers with the highest correlation on each chromosome were surrounded by at least 19 consecutive markers with $R > R_{max} * 0.75$. This filter is very robust and flexible because the 19 neighboring informative markers on each chromosome can be located on one or both sides of the breakpoints and up to several megabases away, allowing detection of IRs even when they affect the telomeres or when they are in runs of homozygosity (RoHs) (Fig. 1C, white bands in the LD heatmap). In case of long RoHs, however, more than 30 progeny might be required to obtain a significant R_{max} if the first informative marker is located >10 Mb from the breakpoint. These large RoHs classically represent >3% of genomes in inbred breeds (Marras et al. 2015).

Another factor that may also contribute to reduced power of detection is the genotyping of a small proportion of aneuploid conceptuses, although in a general manner most of them die during embryogenesis, and the survivors are less likely to be genotyped for genomic evaluation because of their poor appearance. In the case of the bull Nt, the genotyping of a small proportion of calves affected by partial BTA4 mono- or trisomy resulted in imputation and phasing errors, which explains why this sire had the lowest LD max value among confirmed IR carriers. The deletions of several megabases associated with t(24;29)-der 29 and t(3;8) also caused local phasing and imputation errors because of Mendelian transmission errors between hemizygous sires and hemizygous progeny. An example of this can be seen in the LD heat map between the BTA3 and BTA8 markers (Fig. 1D), where a region of low LD corresponding to the deletion site (green) is surrounded by two regions of high LD (red bars).

In any case, LD-based screening for IRs is more sensitive than GTG banding, and we anticipate that its routine use as a by-product of genomic evaluations will allow the

Table 3. Selection of genes affected by IRs

IR	BTA	Gene symbol	Impact of the IR	Phenotypic consequences in model species
t(1;11)	1	*COPB2*	Putative deregulation	M: Decreased body fat mass (Dickinson et al. 2016)
		MRPS22	Putative deregulation	M: Decreased cell proliferation; decreased lean body mass (Dickinson et al. 2016)
	11	*APOB*	Putative deregulation	M: Decreased cholesterol level (Farese et al. 1995) potentially driving to growth delay
t(2;22)	2	*CXCR4*	Putative deregulation	M: Embryonic growth retardation associated with abnormal placentation (Dickinson et al. 2016); various immune defects (Balabanian et al. 2012) H: Immune defect (WHIM syndrome 1) (Beaussant Cohen et al. 2012)
	22	No gene—breakpoint putatively located in centromere		
t(3;8)	3	Six genes	Deleted	No deleterious phenotype reported in heterozygous mutant mice
	8	*FOCAD*	Disrupted	No deleterious phenotype reported in heterozygous mutant mice
		MLLT3	Putative deregulation	H: Growth delay association to reciprocal translocation (Pramparo et al. 2005)
inv ins(8;4)	4	*GARS1*	Putative deregulation	M: Decreased body weight, abnormal gait, muscular atrophy, postnatal growth retardation, premature death, and many others (Seburn et al. 2006; Achilli et al. 2009) H: Charcot–Marie–Tooth disease type 2D and other neuropathies (Antonellis et al. 2003)
		CCM2	Disrupted	H: Cerebral cavernous malformation (Liquori et al. 2007)
	Partial 4 aneuploidy	60 genes including *GARS1*, *HOXA* cluster and *SNX10*	Deletion or trisomy in some offspring	*HOXA* cluster: M: Skeletal development delay (Mark et al. 1997; Pezzani et al. 2015) *SNX10*: H: osteoporosis, postnatal growth retardation (Ye et al. 2015)
	8	*KDM4C*	Putative deregulation	M: Decreased body weight (Ozaki et al. 2015)
t(5;28)	5	*MB*	Putative deregulation	M: Embryonic lethality during organogenesis, incomplete penetrance (Meeson et al. 2001)
		TMPRSS6	Putative deregulation	M: Decreased circulating iron level (Finberg et al. 2010)
	28	No candidate		
t(19;23)	19	*TMEM94*	Putative deregulation	M: Decreased body weight (Dickinson et al. 2016)
		HID1	Disrupted	No deleterious phenotype reported in heterozygous mutant mice
		RPL38	Putative deregulation	M: Decreased body length (Hustert et al. 1996)
	23	*SCUBE3*	Putative deregulation	H: Possible reduced size (Lin et al. 2021)
t(24;29), -der29	24	*CCBE1*	Disrupted	No deleterious phenotype reported in heterozygous mutant mice
		18 genes including *PIGN* and *BCL2*	Deleted	*PIGN*: M: Abnormal development of organs(Dickinson et al. 2016); H: Congenital anomalies, developmental delay (Ohba et al. 2014) *BCL2:* M: Immune defects driving to premature death (Xiang et al. 2011)
	29	11 genes	Deleted	No deleterious phenotype reported in heterozygous mutant mice
		CHORDC1	Putative deregulation	M: Weight loss, premature death (Di Savino et al. 2015; Dickinson et al. 2016)

Selection of genes affected by IRs. This table shows disrupted or deleted genes, as well as a selection of functional candidates that are located upstream of or downstream from the breakpoints within the same TADs, and whose expression may be affected ("putative deregulation"). (M) Phenotypes described in mouse, (H) phenotypes described human.

discovery of even rarer and smaller chromosomal alterations in the future.

Effects on phenotypes and implications for the industry

Taking advantage of the wealth of information available in the French national bovine databases, we investigated the phenotypic effects of IRs on several traits in male carriers and their female offspring.

We observed strong negative effects of the insertional and reciprocal translocations on male fertility, in agreement with previous studies reporting that these types of IR form quadrivalents at meiosis, which after segregation produce relatively high proportions of unbalanced gametes and nonviable embryos. For example, Ogilvie and Scriven (2002) found only 47.7% (71/149) of human embryos with normal or balanced karyotypes in a preimplantation genetic diagnosis study of 18 couples carrying 15 different reciprocal translocations. The fact that the 10 reciprocal translocation carriers were in the worst percentile for the success at first insemination and that they represent 35% of this worst percentile in our study also agrees with the observations of Ducos et al. (2007) in pigs. The latter detected IR in about half of the boars referred to their cytogenetic platform by the breeding organization for hypoprolificacy during the period of 2002–2006. Therefore, our approach adds to the tools set up in the past decade to manage bovine fertility using genomic data (Capitan et al. 2015). In parallel, we recommend that breeding companies consider low NRR as a potential sign of IR and take the necessary steps to verify this hypothesis and stop marketing the semen of these bulls.

It should also be noted that the kinetics of embryo loss varied between bulls. For example, Ma showed an early decrease in NRR compatible with a loss of aneuploid conceptuses at the beginning

of embryogenesis, whereas for Qu, the loss was more progressive and extended over a period covering organogenesis and beyond (see Fig. 3B). We assume that segment size and gene content influence the onset and the penetrance of embryonic lethality, as these two bulls carried one of the largest and smallest reciprocal translocations, respectively. Further supporting this hypothesis, the bull Nt, affected by a small insertional translocation of 11 Mb, was less infertile than carriers of reciprocal translocations, being only in the worst 5% for the success at first insemination. Conversely, it had the highest juvenile mortality rate in our data set, with 44% of females dying between birth and 365 d. We found low proportions of carriers of partial BTA4 trisomy (23%) and monosomy (4%) among its genotyped offspring, indicating that some of them were able to survive until sampling, which is usually performed between 2 and 6 mo of age for routine genomic evaluation. In addition, we showed that these animals had higher mortality rates compared with wild type and balanced controls (Fig. 3D). These results are in line with the recent report by Besnard et al. (2023) of high mortality rates and partial monosomy of the first 37 Mb of BTA29 in the offspring of a bull carrier of a t(26;29) reciprocal translocation, which had a slightly reduced conception rate. Taking all these elements into account, we assume that the higher mortality rates observed for three other IR carriers (in the worst 5%) (see Fig. 3C) are the result of a small proportion of aneuploid births that probably died at an early age or had a particularly poor appearance that prevented their genotyping.

Finally, the rob(18;21) carrier was within the normal range for both male fertility and juvenile mortality. Therefore, we assume that this bull produced only a low proportion of chromosomally unbalanced spermatozoa resulting from adjacent meiotic segregation, that is, possibly ~≤5%, as previously reported, for example, for carriers of rob(1;29), rob(1;21), rob(7;21), and rob(3;16) (Tateno et al. 1994; Bonnet-Garnier et al. 2006; Barasc et al. 2019).

Regarding the consequences of IRs on female offspring, we found significant effects on at least one of the phenotypes studied (age at the first insemination, success at first insemination, and rate of slaughtered animals without calving), except for the bull Sa (t(2;11)), which had the lowest number of phenotyped progeny ($n = 23$). For the latter, we obtained suggestive but not significant effects owing to statistical power limitations. Conversely, the two bulls with the highest number of available phenotypes (Ma and Nt, 506 and 347 complete phenotypes, respectively) showed highly significant differences for all traits studied.

In six of the eight bulls studied, we found that balanced daughters had significantly delayed first inseminations compared with their wild-type sisters, thus supporting growth retardation. This effect, probably because of the disruption, deletion, or deregulation of genes located near the breakpoints (see section "Long-read sequencing and candidate genes"), was not expected as their balanced sires had gone through a selection process to become AI bulls. This calls into question the criteria used to select candidate bulls, which may be more focused on genomic indices and semen quality than on physical appearance. In contrast, the detrimental effects of IRs on the success at first insemination were expected. Indeed, female carriers are predicted to produce rates of unbalanced gametes as high as those of their own sires, resulting in the loss of aneuploid embryos. Our study also provides an overview of the technical consequences of infertility, with a significant increase in the culling of balanced and aneuploidy females before they calve and start their productive life. Of note, the decision to cull an unproductive animal is costly for farmers, as the sale of meat generally does not cover the rearing costs.

In this paper, we have not estimated the financial costs of IRs, but they seem to be colossal. Lewis et al. (2022) proposed an estimation of the cost to the industry. Their estimation reaches US $1.5 million per year per AI bull carrier, based on an average fertility reduction of 10 points and the use of 23,000 semen straws per bull per year (which only Ma and Nt reached in the 12 IRs). In this study, we found higher effects on fertility, with a reduction in conception rates of more than 20 points for most IR carriers (Fig. 3B), and highlighted other deleterious effects on subsequent generations, such as reduced fertility and growth and increased mortality of balanced and aneuploid offspring, which were not considered in the latter estimate. Therefore, the costs estimated by Lewis et al. (2022) are underestimated despite their high level. Finally, in addition to the economic aspects, we would also like to emphasize the negative effects of IRs on animal welfare, on the working conditions of the breeders, and the environmental footprint of livestock production.

In light of these elements, we strongly recommend the early and systematic karyotype screening of future insemination bulls using a GTG banding protocol. As a by-product of genomic selection, our approach provides an easy to implement and very sensitive tool to detect IRs that may be missed by cytogenetic analyses and, most importantly, to track carriers through the generations (e.g., down to great-granddaughters for Fe and Fa) (Supplemental Figs. S1F, S2F) for eradication purposes.

Long-read sequencing and candidate genes

To better characterize IRs, we sequenced the genomes of seven carrier bulls using long-read technology and were able to identify the exact breakpoint locations for six of them. In one case (t(2;22)), we identified the breakpoint on only one chromosome because of the presence of several kilobases of BTSAT2 satellite material, leading us to believe that the breakpoint was located in the centromere of the second chromosome. Thus, our success rate was similar to that of Bouwman et al. (2020), who found breakpoints in six out of seven boars affected by reciprocal translocations using 30× short-read paired-end sequencing. It is worth noting that the *Bos taurus* genome contains a higher proportion of repeated elements (49.4%) than that of *Sus scrofa* (44.5%; http://repeatmasker.org/genomicDatasets/RMGenomicDatasets.html). A posteriori analyses revealed that using short-read sequencing, we would have missed the breakpoint on BTA2 for t(2;22) and also another breakpoint located in repeated elements whose size exceeds that of paired-end inserts (typically 350–500 bp). This was the case for the second breakpoint of t(3;8) in BTA3, which was located in a 3-kb segment consisting of three long interspersed nuclear elements (LINEs), a short interspersed nuclear element (SINE), and a long terminal repeat sequence (LTR). It is also likely that we would have missed other features of the IRs studied, such as a 6-kb inversion at the fusion point of BTA24 for t(24;29),-der29 (Table 2), without the reconstruction of local alignments with nucleotide resolution around the breakpoints made possible by long-read sequencing technology.

We then sought to explain the phenotypic differences observed between wild-type and affected progeny by analyzing the function of the genes located on and around the breakpoints.

For only two of seven IRs, we found convincing disrupted or deleted functional candidates (Table 3). Regarding t(24;29),-der29, heterozygous mutations in *PIGN* have been associated with developmental delay and progressive cerebellar atrophy in human (Ohba et al. 2014) and mice (Dickinson et al. 2016). In addition, *BCL2*

haploinsufficiency was found to cause premature death in mouse. All affected animals died before 2 yr of age, compared with only 20% for wild-type animals (Xiang et al. 2011). For the inv ins(8;4), mutations in *CCM2* are responsible for dominant defects of brain vascularization in humans (Liquori et al. 2007) and in mice (Plummer et al. 2006), leading to an increased risk of hemorrhagic stroke and seizures. This could explain the 2.5-fold higher juvenile mortality rate in the balanced compared with wild-type heifers.

In addition to the disrupted and deleted genes, we identified 12 genes located upstream of or downstream from the breakpoints whose expression may be affected by the alteration of the TAD boundaries and that have been associated with deleterious phenotypes in haploinsufficient mice and/or humans. Among them, *GARS1*, which is located in the segment of BTA4 inserted into BTA8 (inv ins(8;4) in bull Nt) at only 60 kb from the most proximal breakpoint, caught our attention. Numerous heterozygous mutations of this gene have been identified in human patients affected by Charcot–Marie-Tooth disease, type 2D, and other neuropathies, the most severe form of which is infantile spinal muscular atrophy, James type (Antonellis et al. 2003; James et al. 2006; Forrester et al. 2020). Similar observations have been made in the mouse with reports of muscle atrophy, decreased body weight, and premature death in heterozygotes for several different variants (Seburn et al. 2006; Achilli et al. 2009; Dickinson et al. 2016). Therefore, in addition to *CCM2* disruption, *GARS1* down-regulation may also contribute to the retarded growth and high mortality rate of balanced daughters (see Fig. 3D; Supplemental Fig. S7K). Together with untolerated aneuploidy, some of the putatively deregulated genes may also increase embryonic lethality and partially explain the very low level of fertility of IR carriers (see Fig. 3A,B; Supplemental Table S1). For example, the gene *MB*, located at 562 kb from the BTA5 breakpoint of t(5;28), has been identified in mice as causing embryonic lethality at the organogenesis stage in heterozygous mutant embryos (Meeson et al. 2001).

Regarding the putative causes of reduced survival in aneuploid progeny, we would like to mention that the 11-Mb segment of BTA4, for which we observed live monosomic and trisomic progeny, contains 60 genes, including 11 members of the *HOXA* cluster. *Hox* genes are key determinants of the identity of the morphological segments of each body part along the anteroposterior axis in most bilaterians (Hughes and Kaufman 2002; Mallo and Alonso 2013), and their deletion, duplication, or ectopic expression has been shown to cause a wide variety of body plan modifications in numerous species, including domestic animals (e.g. chicken, goat, and sheep, to name a few) (Wang et al. 2012; Allais-Bonnet et al. 2021). Haploinsufficiency for the *HOXA* gene cluster may be the cause of limb malformations reported in two progeny of the bull Nt (carrier of the inv ins(8;4)) that were euthanized at birth several months before the start of this study. In addition to *GARS1* and *CCM2* previously presented above, *SNX10* haploinsufficiency could also contribute to the higher mortality rate of monosomic offspring of Nt between genotyping and the first year of life and to their significant underrepresentation, supporting prenatal or early juvenile mortality. Indeed, mice heterozygous for a mutation in *SNX10* were found to display postnatal growth retardation (Ye et al. 2015). This matches with the high delay at first insemination age and with the developmental delay observed in a partially monosomic female (Supplemental Fig. S7K). Note that trisomic females have also been described as having delayed growth (M. Van Berghe, pers. comm.).

To conclude this section, the combination of analyses of large phenotype data sets with long-read sequencing and functional annotations suggests that most of the rearrangements have deleterious consequences in balanced animals even in the absence of direct deletion or disruption of candidate genes. Although further analyses are needed to describe the mechanisms involved, the IRs we identified are interesting models for studying gene regulation and the organization of genome structure.

Search for specific characteristics of IR

Throughout this study, we have attempted to highlight specific characteristics of IR in order to contribute to a better understanding of the processes responsible for their occurrence. Despite our limited data set, we obtained encouraging results. For example, we determined that 11 of the 12 detected IRs were caused by female ($n = 1$) and male ($n = 10$) meiotic defects. This result is consistent with observations in humans, where it has been found that 87% of unequal crossing-overs resulting in a viable conceptus occur in male meiosis (Shaffer and Lupski 2000).

We also observed a significant overrepresentation of the breakpoints in the third-quarter of the chromosomes ($P < 0.04$). At this stage, we do not have any explanations to propose to explain this phenomenon because this region did not show higher recombination rates in the general population (Supplemental Fig. S14), and the breakpoints did not colocalize with recombination hotspots based on LD analyses in the progeny of the bulls that produced the mutant gametes.

Furthermore, by analyzing long-read sequences, we did not identify any redundant repeat elements or specific motifs around the breakpoints that could have promoted the occurrence of IRs. In fact, we found repeat elements of various types in about half of the breakpoints, which is not unlikely considering that such DNA material makes up 49.4% of the bovine genome. The sire's age at conception had no effect, as also reported by Sloter et al. (2004) in a review of human and mouse sperm production. Finally, we found no significant increase in chromosome or chromosome pair representation in our reduced data set of 12 IRs. Taken together, these results suggest that IRs are a random process with an increased risk of occurring during male gametogenesis following intense meiotic activity. However, the question of the existence of genetic predisposition factors remains, which was raised by the observation of two carriers of different reciprocal translocations out of 48 sons of a single elite sire (t(5;28) and t(2;22) in the bulls Fa and Fe, respectively). We have no doubt that such a question will be answered as our easy-to-implement approach is applied to other populations and species and as an increasing number of well-characterized IRs will accumulate.

In conclusion, our results show the value of the large genotypic, pedigree, and phenotypic data sets generated by routine genomic evaluations in cattle to detect IRs and characterize their phenotypic consequences. LD-based screening for IRs is readily applicable to any population that benefits from similar data sets, and will have direct applications in plant and animal breeding. This approach also offers interesting prospects in terms of basic research, by allowing the detection of smaller and rarer types of chromosomal rearrangements than those identified by GTG banding, which are interesting models for studying gene regulation and the organization of genome structure.

Methods

Screening for IRs using SNP array genotypes

Genotypes

The initial data set consisted of 1,749,746 cattle from 15 breeds that were genotyped together with their sire using various Illumina SNP arrays over time (LD, ~7 K SNPs; custom LD, ~10 K to 20 K; BovineSNP50, ~50 K; EuroGMD, ~63 K; and HD, ~777 K). Raw genotypes were imputed and phased for 44,307 autosomal SNPs by FImpute (Sargolzaei et al. 2014) as part of the French routine genomic evaluation of cattle, as described by Mesbah-Uddin et al. (2019).

Simulation

To estimate significance thresholds for LD between pairs of markers from different chromosomes, we developed a specific simulation procedure. One hundred AI bulls were selected based on their large number of genotyped progeny ($n \geq 1500$) and phenotypic information suggesting that they were free of IR (percentiles 11 to 89 for conception rate and juvenile mortality). For each sire, 100 samples of n offspring were randomly drawn, resulting in 10,000 simulations for a given n. LD was calculated between pairs of markers from different chromosomes using the R (R Core Team 2021) package gaston 1.5.7 (https://cran.r-project.org/package=gaston) and map information from the ARS-UCD1.2 bovine genome assembly. The highest LD value (absolute correlation between alleles, also called R_{max}) was scored for each simulation. To avoid spurious and punctual LD, we retained R_{max} only if the two markers with the highest correlation were surrounded by at least 19 consecutive markers with $R > R_{max} * 0.75$. The 10th highest R_{max} found in the 10,000 simulations was taken as the threshold value for $P < 0.001$. We chose a false-discovery rate of 1‰, which is slightly lower than the prevalence of IR reported in two large studies focusing on phenotypically normal and fertile males of the human (2.06‰) (Ravel et al. 2006) and pig (4.7‰) (Ducos et al. 2007) species, in order to limit false positives.

The same process was repeated for 12 values of n ($n = 25$, 30, 40, 50, 60, 80, 100, 200, 350, 500, 750, and 1000), and a regression curve was fitted to obtain the appropriate threshold for each number of progeny per bull.

Screening of the population

To detect putative rearrangements in the population, we followed the same procedure as for simulations and calculated LD in 5571 paternal half-sib families with more than 30 progeny (mean = 292 ± 565 individuals; max = 13,347) (Supplemental Table S2). Thirty was found to be the minimum number of progeny to reach a significant LD ($P < 0.001$) based on simulation results. On average, 14,561 ± 607 markers per sire family were considered to be informative (i.e., heterozygous in the sire and with a minor allele frequency set at 20% in the paternal phases of the progeny; this rate allows avoidance of imputation errors and was fixed using data from the same bull's progeny as in the simulations). To be considered as significant, the LD values between pairs of markers from different chromosomes had to exceed the threshold determined by the equation obtained by simulation: $y = 4.0302x^{-0.0408}$ (where x is the number of progeny). Analyses were performed on 1000 randomly selected offspring when the number of genotyped progeny exceeded this threshold. For more details on the available material, see Supplemental Table S2.

Finally, it should be noted that Chromosome X has not been considered in this study for two reasons. First, markers from the X-specific region are hemizygous in the sires and therefore not informative in paternal half-sib families, and, second, there is a sex ratio bias in the genotyped progeny with an average of 92% of females, which would affect calculations for markers located on the pseudoautosomal region.

Cytogenetic analyses

To verify our findings based on LD, we conducted a series of cytogenetic analyses on the bulls themselves (for bull Ma), their daughters (for bulls Im, Ja, Le, Nt, No, Ob, Ou, Qu, Ra, and Sa), or even their granddaughters (for bulls Fa and Fe) depending on the availability of material at the time of the study. Among the descendants of a bull, our goal was to sample at least two carrier and two noncarrier progeny of the haplotypic combination observed around the putative breakpoints. A total of 42 animals were included in these analyses. At first, we studied the karyotypes observed in metaphase II and stained by GTG banding. These were obtained from blood lymphocytes as described by Ducos et al. (1998). Breakpoints were estimated according to the standard GTG banded bovine karyotype (Cribiu et al. 2001).

In two cases, the GTG banding resolution (5–10 Mb) was not sufficient, and we performed FISH with chromosome-specific DNA painting probes to confirm the rearrangements and highlight cases of aneuploidy. Skin biopsies were obtained from ear punches. Fibroblast cultures and metaphases were obtained according to the method of Ducos et al. (2000b). For the inv ins(8;4) rearrangement, the nucleotide sequences of the segments adjacent to the breakpoints were aligned against bovine bacterial artificial chromosome (BAC) end sequences using BLAST (http://blast.ncbi.nlm.nih.gov/Blast.cgi, last accessed January 24, 2022). Two INRA BAC clones were selected and obtained from the biological resources of the @BRIDGe facilities (http://abridge.inrae.fr): CH240-444F5, targeting the segment deleted on BTA4, and CH240-267G16, targeting the centromeric region of BTA8 that is duplicated and inserted in BTA4. FISH experiments were performed according to the method of Yerle et al. (1994). The two BACs were labeled with biotin and digoxygenin, respectively, using the BioPrime DNA labeling system kit (Invitrogen). Finally, they were revealed by Alexa Fluor 594 conjugated to streptavidin (Molecular Probes S32356A) and FITC conjugated mouse antidigoxygenin antibodies (Sigma-Aldrich F3523).

For the reciprocal translocation involving BTA24 and BTA29, an INRA BAC clone targeting the centromeric regions of the acrocentric chromosomes was selected: CH240-369L1. This BAC was also labeled with biotin using the BioPrime DNA labeling system kit (Invitrogen) and then revealed with Alexa Fluor 594 streptavidin (Molecular Probes).

Age of sire at conception

For 10 IRs resulting from abnormal male meiosis, we calculated the age of the sires at conception of their first mutant carriers. In parallel, we calculated their mean age at conception of their wild-type progeny ($n = 118$ in total) available in our initial screen of 5571 bulls. Finally, we compared the means of the two groups using a Student's t-test. For the sire of bulls Fa and Fe, the control group was randomly split in two.

Haplotype tests

To predict the status of the genotyped progeny of IR carrier bulls and to trace the affected segments in their pedigrees, we developed haplotype tests using 10 informative SNPs on each chromosome. These were chosen to be as close as possible to the breakpoints when sequence information was available or, by default, to retain

the highest LD values between markers from nonhomologous chromosomes.

Phenotypic effects of IR

To characterize the phenotypic effects of IR, a variety of information was obtained from the French national bovine databases. In addition to individual ID, sex, pedigree, and herd, these data included information on insemination (date, female and male ID) and other life events such as dates of birth, death, and sale, as well as cause of death (natural or slaughter). Only records between January 1, 2010, and July 31, 2022, were considered. Conception and NRRs were calculated for IR carriers and for 2900 wild-type bulls (based on our initial screen for IR) with at least 100 registered AIs, and expressed as standard deviations from the mean of their breed to allow compilation of results from different breeds. Only first inseminations within parity (i.e., the first AI for heifers or the first AI after each calving for adult cows) performed with conventional semen were included, resulting in a total of 26,372,760 AI records. AIs were considered successful if calving occurred between 265 and 295 d later, unsuccessful if the calving occurred after 295 d, and filtered out if the female died before 295 d. NRRs after *n* days were scored as one if no subsequent insemination occurred within *n* days after and as zero otherwise. Mortality rates per bull were calculated as the number of females that died before 365 d of age divided by the number of females born and then expressed as standard deviations from the mean of their breed.

Additional indicators were calculated for eight IR carriers that had at least 20 genotyped and inseminated daughters. In the absence of routine growth recording in dairy heifers, we used age at insemination as a proxy, as it is generally recommended to inseminate Holstein heifers at 380–400 kg (i.e., ~60% of adult liveweight) (Le Cozler et al. 2008). Finally, the proportion of females slaughtered without calving was calculated as the number of heifers alive at 20 mo that were later slaughtered without a calving record divided by the total number of daughters alive at 20 mo.

Long-read sequencing

DNA extraction

DNA from seven IR-affected bulls was extracted from 200-µL semen straws using the Gentra Puregene tissue kit (Qiagen). The straws were rinsed with 1 mL of PBS 1× buffer, and the resulting solutions were centrifuged for 5 min at 21,130*g* at room temperature. The sperm pellets were resuspended in 500 µL of Qiagen RLT buffer containing 50 mM of Tris(2-carboxyethyl)phosphine hydrochloride (TCEP; pH = 7), before adding 500 µL of nuclei lysis solution and incubating for 3 hours at 55°C with slow shaking. The lysates were then cooled for 5 min on ice before 200 µL of protein precipitation solution was added, and they were incubated for a further 5 min on ice. After 10 sec of vigorous vortexing, the proteins were pelleted by centrifugation at 21,130*g* for 5 min. The supernatants were then transferred to clean tubes containing 600 µL of isopropanol. DNA pellets were obtained by gently inverting the tubes, centrifuging at 21,130*g* for 5 min, rinsing in 70% ethanol, and resuspending in TE buffer.

PacBio CLR sequencing

Library preparation and sequencing were performed at the INRAE GeT-PlaGe core facility in Toulouse (https://get.genotoul.fr/la-plateforme/get-plage/) according to the manufacturer's instructions (procedure & checklist–preparing HiFi SMRTbell libraries using the SMRTbell express template prep kit 2.0). At each step, DNA samples were purified using AMPure PB beads (PacBio), and DNA concentration, purity, size distribution, and degradation were assessed using a Qubit fluorometer (Thermo Fisher Scientific), a NanoDrop spectrophotometer (Thermo Fisher Scientific), and a Femto pulse system (Agilent), respectively. For each library, 10 µg of high-molecular-weight DNA was sheared to ~30 kb using the Megaruptor3 system (Diagenode). Single-strand overhangs were removed, and DNA fragments were damage-repaired using the SMRTbell express template prep kit 2.0. Blunt hairpin adapters were ligated to the library. Fragments of ~10–15 kb were filtered using the BluePippin size selection system (Sage Science). The SMRTbell libraries were annealed (1 h) and bound (4 h) with sequencing primer v5 and the Sequel II DNA Polymerase 2.0 from the Sequel II binding kit 2.0. The final sample-bound complexes were sequenced on a Sequel II instrument (PacBio) using one SMRT cell each and the sequencing kit 2.0 (loading concentration of 80 to 90 pM, movie time of 15 h). On average, a mean CLR coverage of 58× and a mean UMY coverage of 32× were obtained for the seven genomes.

Sequence analysis

Reads were aligned to the bovine ARS-UCD1.2 reference assembly (https://www.ncbi.nlm.nih.gov/data-hub/genome/GCF_002263795.1/) using the pbmm2 software (https://github.com/PacificBiosciences/pbmm2), and structural variations were detected using pbsv (https://github.com/PacificBiosciences/pbsv). The translocation breakpoints were identified as breakend (BND) records, which document the two breakends of a new adjacency (i.e., an adjacency not present in the reference genome; https://samtools.github.io/hts-specs/VCFv4.3.pdf). To confirm and characterize the different rearrangements at the nucleotide level, local (haplotype resolved) assemblies were constructed. For each new adjacency, the corresponding chimeric reads were extracted and assembled using the flye software (Kolmogorov et al. 2019). These assemblies were used to characterize the breakpoint region in more detail. Finally, the Integrative Genomics Viewer (IGV) v2.15.2 (Thorvaldsdóttir et al. 2013) was used to visualize the reads supporting the existence of IR.

Annotation

Various sources of information were used to annotate the genomic regions affected by the break points and fusion points and to predict the putative consequences of the rearrangements on neighboring genes. These included Ensembl (v108) annotated genes extracted using BioMart (https://www.ensembl.org/biomart/martview/), repeat elements available in the UCSC Genome Browser (https://genome-euro.ucsc.edu/; track "Repeat elements by RepeatMasker"), clinical signs reported in mutants from different species (human, https://www.omim.org; mouse, https://www.informatics.jax.org; and other animals, https://omia.org/), and, finally, a map of bovine TADs predicted by synteny with other mammals (Wang et al. 2018). For the latter, we used the UCSC liftOver tool (https://genome.ucsc.edu/cgi-bin/hgLiftOver) to convert positions from the UMD3.1 to the ARS-UCD1.2 bovine genome assembly. The list of genes obtained is available in Supplemental Table S5.

Recombination hotspots

We estimated the locations of recombination hotspots using the same LD as in the previous part of the Methods section. We considered the closest informative markers (i.e., heterozygous) surrounding breakpoints found in sequences in the sires of bulls affected by a meiotic-origin IR. The LD between these two SNPs was then compared with the LD along the affected chromosome in the same

progeny cohort. The SNPs considered for the comparison were at similar distances as the two informative neighboring SNPs around the breakpoints (±10%).

To compare rearrangement positions with LD along a theoretical chromosome, we used LD computed in simulations and plotted it, expressing chromosome-wide positions as a percentage of their physical position (for more details, see Supplemental Fig. S14).

Data access

The long-read sequences data generated in this study have been submitted to the European Nucleotide Archive (ENA; https://www.ebi.ac.uk/ena/browser/home) under accession number PRJEB59364. The genotype data used in this study have been submitted to the Recherche Data Gouv (https://entrepot.recherche.data.gouv.fr/) under the DOI https://doi.org/10.57745/ELW696. No accession number is required.

Competing interest statement

The authors declare no competing interests.

Acknowledgments

We thank the many breeders, veterinarians, agricultural technicians, and breeding companies involved in this study for providing blood, semen samples, and phenotypic information. We also thank @BRIDGe for providing BAC clones. Finally, we thank the members of the *SeqOccIn* Consortium for their valuable help and advice (i.e., Camille Eché, Christine Gaspin, Clément Birbes, Andreea Dreau, Quentin Boone, Christophe Klopp, Matthias Zytnicki, and Denis Milan from INRAE, the Genotoul GeT-PlaGe facility, or the Genotoul Bioinformatics facility). J.J. is supported by a CIFRE PhD grant from Eliance, with financial support from the Association Nationale de la Recherche et de la Technologie and APIS-GENE (Paris, France). This study was also supported by the *Fertiligest* and *Effitness* projects funded by APIS-GENE and by the *SeqOccIn* project cofunded by the European Union and the Occitania Region (FEDER-FSE MIDI-PYRENEES ET GARONNE 2014-2020).

Author contributions: A.Cap. and J.J. conceived the study with insights from H.B., A.P., and D.B. on specific points. H.B., A.Cal., N.B., and A.P. performed the cytogenetic analyses. J.J., S.T., F.B., A.B., C.H., and A.Cap. analyzed the genotypic and phenotypic data. C.M., A.S., C.K., C.I., C.D., and C.G. participated in DNA extraction, library preparation, and long-read sequencing. T.F., J.J., and A.Cap. analyzed long-read sequences. J.J. and A.Cap. wrote the manuscript with input from all the coauthors.

References

Achilli F, Bros-Facer V, Williams HP, Banks GT, AlQatari M, Chia R, Tucci V, Groves M, Nickols CD, Seburn KL, et al. 2009. An ENU-induced mutation in mouse glycyl-tRNA synthetase (*GARS*) causes peripheral sensory and motor phenotypes creating a model of Charcot-Marie-Tooth type 2D peripheral neuropathy. *Dis Model Mech* **2:** 359–373. doi:10.1242/dmm.002527

Allais-Bonnet A, Hintermann A, Deloche M-C, Cornette R, Bardou P, Naval-Sanchez M, Pinton A, Haruda A, Grohs C, Zakany J, et al. 2021. Analysis of polycerate mutants reveals the evolutionary co-option of *HOXD1* for horn patterning in Bovidae. *Mol Biol Evol* **38:** 2260–2272. doi:10.1093/molbev/msab021

Antonellis A, Ellsworth RE, Sambuughin N, Puls I, Abel A, Lee-Lin S-Q, Jordanova A, Kremensky I, Christodoulou K, Middleton LT, et al. 2003. Glycyl tRNA synthetase mutations in Charcot-Marie-Tooth disease type 2D and distal spinal muscular atrophy type V. *Am J Hum Genet* **72:** 1293–1299. doi:10.1086/375039

Balabanian K, Brotin E, Biajoux V, Bouchet-Delbos L, Lainey E, Fenneteau O, Bonnet D, Fiette L, Emilie D, Bachelerie F. 2012. Proper desensitization of *CXCR4* is required for lymphocyte development and peripheral compartmentalization in mice. *Blood* **119:** 5722–5730. doi:10.1182/blood-2012-01-403378

Barasc H, Mouney-Bonnet N, Peigney C, Calgaro A, Revel C, Mary N, Ducos A, Pinton A. 2019. Analysis of meiotic segregation pattern and interchromosomal effects in a bull heterozygous for a 3/16 Robertsonian translocation. *Cytogenet Genome Res* **156:** 197–203. doi:10.1159/000494289

Beaussant Cohen S, Fenneteau O, Plouvier E, Rohrlich P-S, Daltroff G, Plantier I, Dupuy A, Kerob D, Beaupain B, Bordigoni P, et al. 2012. Description and outcome of a cohort of 8 patients with WHIM syndrome from the French Severe Chronic Neutropenia Registry. *Orphanet J Rare Dis* **7:** 71. doi:10.1186/1750-1172-7-71

Besnard F, Leclerc H, Boussaha M, Grohs C, Jewell N, Pinton A, Barasc H, Jourdain J, Femenia M, Dorso L, et al. 2023. Detailed analysis of mortality rates in the female progeny of 1,001 Holstein bulls allows the discovery of new dominant genetic defects. *J Dairy Sci* **106:** 439–451. doi:10.3168/jds.2022-22365

Bonnet-Garnier A, Pinton A, Berland HM, Khireddine B, Eggen A, Yerle M, Darré R, Ducos A. 2006. Sperm nuclei analysis of 1/29 Robertsonian translocation carrier bulls using fluorescence in situ hybridization. *Cytogenet Genome Res* **112:** 241–247. doi:10.1159/000089877

Bourneuf E, Otz P, Pausch H, Jagannathan V, Michot P, Grohs C, Piton G, Ammermüller S, Deloche M-C, Fritz S, et al. 2017. Rapid discovery of de novo deleterious mutations in cattle enhances the value of livestock as model species. *Sci Rep* **7:** 11466. doi:10.1038/s41598-017-11523-3

Bouwman AC, Derks MFL, Broekhuijse MLWJ, Harlizius B, Veerkamp RF. 2020. Using short read sequencing to characterise balanced reciprocal translocations in pigs. *BMC Genom* **21:** 576. doi:10.1186/s12864-020-06989-x

Burssed B, Zamariolli M, Bellucco FT, Melaragno MI. 2022. Mechanisms of structural chromosomal rearrangement formation. *Mol Cytogenet* **15:** 23. doi:10.1186/s13039-022-00600-6

Capitan A, Michot P, Baur A, Saintilan R, Hozé C, Valour D, Guillaume F, Boichon D, Barbat A, Boichard D, et al. 2015. Genetic tools to improve reproduction traits in dairy cattle. *Reprod Fertil Dev* **27:** 14–21. doi:10.1071/RD14379

Clementini E, Palka C, Iezzi I, Stuppia L, Guanciali-Franchi P, Tiboni GM. 2005. Prevalence of chromosomal abnormalities in 2078 infertile couples referred for assisted reproductive techniques. *Hum Reprod* **20:** 437–442. doi:10.1093/humrep/deh626

Cribiu EP, Di Berardino D, Di Meo GP, Eggen A, Gallagher DS, Gustavsson I, Hayes H, Iannuzzi L, Popescu CP, Rubes J, et al. 2001. International System for Chromosome Nomenclature of Domestic Bovids (ISCNDB 2000). *Cytogenet Cell Genet* **92:** 283–299. doi:10.1159/000056917

De Lorenzi L, Morando P, Planas J, Zannotti M, Molteni L, Parma P. 2012. Reciprocal translocations in cattle: frequency estimation. *J Anim Breed Genet* **129:** 409–416. doi:10.1111/j.1439-0388.2011.00983.x

Dickinson ME, Flenniken AM, Ji X, Teboul L, Wong MD, White JK, Meehan TF, Weninger WJ, Westerberg H, Adissu H, et al. 2016. High-throughput discovery of novel developmental phenotypes. *Nature* **537:** 508–514. doi:10.1038/nature19356

Di Savino A, Panuzzo C, Rocca S, Familiari U, Piazza R, Crivellaro S, Carrà G, Ferretti R, Fusella F, Giugliano E, et al. 2015. Morgana acts as an oncosuppressor in chronic myeloid leukemia. *Blood* **125:** 2245–2253. doi:10.1182/blood-2014-05-575001

Ducos A, Berland HM, Pinton A, Guillemot E, Seguela A, Blanc MF, Darre A, Darre R. 1998. Nine new cases of reciprocal translocation in the domestic pig (*Sus scrofa domestica* L.). *J Hered* **89:** 136–142. doi:10.1093/jhered/89.2.136

Ducos A, Berland HM, Pinton A, Seguela A, Brun-Baronnat C, Darre A, Darre R. 2000a. Contrôle chromosomique des populations animales d'élevage. *INRAE Prod Anim* **13:** 25–35. doi:10.20870/productions-animales.2000.13.1.3765

Ducos A, Dumont P, Séguéla A, Pinton A, Berland H, Brun-Baronnat C, Darré A, Marquant-Le Guienne B, Humblot P, Boichard D, et al. 2000b. A new reciprocal translocation in a subfertile bull. *Genet Sel Evol* **32:** 589–598. doi:10.1186/1297-9686-32-6-589

Ducos A, Berland H-M, Bonnet N, Calgaro A, Billoux S, Mary N, Garnier-Bonnet A, Darré R, Pinton A. 2007. Chromosomal control of pig populations in France: 2002–2006 survey. *Genet Sel Evol* **39:** 583–597. doi:10.1186/1297-9686-39-5-583

Farese RV, Ruland SL, Flynn LM, Stokowski RP, Young SG. 1995. Knockout of the mouse apolipoprotein B gene results in embryonic lethality in homozygotes and protection against diet-induced hypercholesterolemia in heterozygotes. *Proc Natl Acad Sci* **92:** 1774–1778. doi:10.1073/pnas.92.5.1774

Finberg KE, Whittlesey RL, Fleming MD, Andrews NC. 2010. Down-regulation of Bmp/Smad signaling by *Tmprss6* is required for maintenance of systemic iron homeostasis. *Blood* **115:** 3817–3826. doi:10.1182/blood-2009-05-224808

Forabosco A, Percesepe A, Santucci S. 2009. Incidence of non-age-dependent chromosomal abnormalities: a population-based study on 88965 amniocenteses. *Eur J Hum Genet* **17:** 897–903. doi:10.1038/ejhg.2008.265

Forrester N, Rattihalli R, Horvath R, Maggi L, Manzur A, Fuller G, Gutowski N, Rankin J, Dick D, Buxton C, et al. 2020. Clinical and genetic features in a series of eight unrelated patients with neuropathy due to Glycyl-tRNA synthetase (*GARS*) variants. *J Neuromuscul Dis* **7:** 137–143. doi:10.3233/JND-200472

Gekas J, Thepot F, Turleau C, Siffroi JP, Dadoune JP, Briault S, Rio M, Bourouillou G, Carré-Pigeon F, Wasels R, et al. 2001. Chromosomal factors of infertility in candidate couples for ICSI: an equal risk of constitutional aberrations in women and men. *Hum Reprod* **16:** 82–90. doi:10.1093/humrep/16.1.82

Hughes CL, Kaufman TC. 2002. Hox genes and the evolution of the arthropod body plan. *Evol Dev* **4:** 459–499. doi:10.1046/j.1525-142X.2002.02034.x

Hustert E, Scherer G, Olowson M, Guénet JL, Balling R. 1996. *Rbt* (rabo torcido), a new mouse skeletal mutation involved in anteroposterior patterning of the axial skeleton, maps close to the *ts* (tail-short) locus and distal to the *sox9* locus on chromosome 11. *Mamm Genome* **7:** 881–885. doi:10.1007/s003359900261

Iannuzzi A, Parma P, Iannuzzi L. 2021. Chromosome abnormalities and fertility in domestic bovids: a review. *Animals (Basel)* **11:** 802. doi:10.3390/ani11030802

James PA, Cader MZ, Muntoni F, Childs A-M, Crow YJ, Talbot K. 2006. Severe childhood SMA and axonal CMT due to anticodon binding domain mutations in the *GARS* gene. *Neurology* **67:** 1710–1712. doi:10.1212/01.wnl.0000242619.52335.bc

Kastelic J, Thundathil J. 2008. Breeding soundness evaluation and semen analysis for predicting bull fertility. *Reprod Domest Anim* **43:** 368–373. doi:10.1111/j.1439-0531.2008.01186.x

Kolmogorov M, Yuan J, Lin Y, Pevzner PA. 2019. Assembly of long, error-prone reads using repeat graphs. *Nat Biotechnol* **37:** 540–546. doi:10.1038/s41587-019-0072-8

Le Cozler Y, Lollivier V, Lacasse P, Disenhaus C. 2008. Rearing strategy and optimizing first-calving targets in dairy heifers: a review. *Animal* **2:** 1393–1404. doi:10.1017/S1751731108002498

Lewis NM, Canedo-Ribeiro C, Rathje CC, Jennings RL, Danihel M, Bosman LM, Silvestri G, Griffin DK. 2022. The economic burden of chromosome translocations and the benefits of enhanced screening for cattle breeding. *Animals (Basel)* **12:** 1982. doi:10.3390/ani12151982

Lin Y-C, Niceta M, Muto V, Vona B, Pagnamenta AT, Maroofian R, Beetz C, van Duyvenvoorde H, Dentici ML, Lauffer P, et al. 2021. SCUBE3 loss-of-function causes a recognizable recessive developmental disorder due to defective bone morphogenetic protein signaling. *Am J Hum Genet* **108:** 115–133. doi:10.1016/j.ajhg.2020.11.015

Liquori CL, Berg MJ, Squitieri F, Leedom TP, Ptacek L, Johnson EW, Marchuk DA. 2007. Deletions in *CCM2* are a common cause of cerebral cavernous malformations. *Am J Hum Genet* **80:** 69–75. doi:10.1086/510439

Mallo M, Alonso CR. 2013. The regulation of Hox gene expression during animal development. *Development* **140:** 3951–3963. doi:10.1242/dev.068346

Mark M, Rijli FM, Chambon P. 1997. Homeobox genes in embryogenesis and pathogenesis. *Pediatr Res* **42:** 421–429. doi:10.1203/00006450-199710000-00001

Marras G, Gaspa G, Sorbolini S, Dimauro C, Ajmone-Marsan P, Valentini A, Williams JL, Macciotta NPP. 2015. Analysis of runs of homozygosity and their relationship with inbreeding in five cattle breeds farmed in Italy. *Anim Genet* **46:** 110–121. doi:10.1111/age.12259

Matveevsky S, Kolomiets O, Bogdanov A, Alpeeva E, Bakloushinskaya I. 2020. Meiotic chromosome contacts as a plausible prelude for Robertsonian translocations. *Genes (Basel)* **11:** 386. doi:10.3390/genes11040386

Meeson AP, Radford N, Shelton JM, Mammen PP, DiMaio JM, Hutcheson K, Kong Y, Elterman J, Williams RS, Garry DJ. 2001. Adaptive mechanisms that preserve cardiac function in mice without myoglobin. *Circ Res* **88:** 713–720. doi:10.1161/hh0701.089753

Mesbah-Uddin M, Hoze C, Michot P, Barbat A, Lefebvre R, Boussaha M, Sahana G, Fritz S, Boichard D, Capitan A. 2019. A missense mutation (p.Tyr452Cys) in the *CAD* gene compromises reproductive success in French normande cattle. *J Dairy Sci* **102:** 6340–6356. doi:10.3168/jds.2018-16100

Ogilvie CM, Scriven PN. 2002. Meiotic outcomes in reciprocal translocation carriers ascertained in three-day human embryos. *Eur J Hum Genet* **10:** 801–806. doi:10.1038/sj.ejhg.5200895

Ohba C, Okamoto N, Murakami Y, Suzuki Y, Tsurusaki Y, Nakashima M, Miyake N, Tanaka F, Kinoshita T, Matsumoto N, et al. 2014. *PIGN* mutations cause congenital anomalies, developmental delay, hypotonia, epilepsy, and progressive cerebellar atrophy. *Neurogenetics* **15:** 85–92. doi:10.1007/s10048-013-0384-7

Ozaki Y, Fujiwara K, Ikeda M, Ozaki T, Terui T, Soma M, Inazawa J, Nagase H. 2015. The oncogenic role of *GASC1* in chemically induced mouse skin cancer. *Mamm Genome* **26:** 591–597. doi:10.1007/s00335-015-9592-9

Pezzani L, Milani D, Manzoni F, Baccarin M, Silipigni R, Guerneri S, Esposito S. 2015. *HOXA* genes cluster: clinical implications of the smallest deletion. *Ital J Pediatr* **41:** 31. doi:10.1186/s13052-015-0137-3

Plummer NW, Squire TL, Srinivasan S, Huang E, Zawistowski JS, Matsunami H, Hale LP, Marchuk DA. 2006. Neuronal expression of the *Ccm2* gene in a new mouse model of cerebral cavernous malformations. *Mamm Genome* **17:** 119–128. doi:10.1007/s00335-005-0098-8

Poornima S, Daram S, Devaki RK, Qurratulain H. 2020. Chromosomal abnormalities in couples with primary and secondary infertility: genetic counseling for assisted reproductive techniques (ART). *J Reprod Infertil* **21:** 269–274. doi:10.18502/jri.v21i4.4331

Poot M, Haaf T. 2015. Mechanisms of origin, phenotypic effects and diagnostic implications of complex chromosome rearrangements. *Mol Syndromol* **6:** 110–134. doi:10.1159/000438812

Popescu PC. 1989. *Cytogénétique des mammifères d'élevage*. INRAE, Paris.

Pramparo T, Grosso S, Messa J, Zatterale A, Bonaglia MC, Chessa L, Balestri P, Rocchi M, Zuffardi O, Giorda R. 2005. Loss-of-function mutation of the *AF9/MLLT3* gene in a girl with neuromotor development delay, cerebellar ataxia, and epilepsy. *Hum Genet* **118:** 76–81. doi:10.1007/s00439-005-0004-1

Ravel C, Berthaut I, Bresson JL, Siffroi JP, the Genetics Commission of the French Federation of 818 CECOS. 2006. Prevalence of chromosomal abnormalities in phenotypically normal and fertile adult males: large-scale survey of over 10,000 sperm donor karyotypes. *Hum Reprod* **21:** 1484–1489. doi:10.1093/humrep/del024

R Core Team. 2021. *R: a language and environment for statistical computing*. R Foundation for Statistical Computing, Vienna. https://www.R-project.org/.

Sargolzaei M, Chesnais JP, Schenkel FS. 2014. A new approach for efficient genotype imputation using information from relatives. *BMC Genom* **15:** 478. doi:10.1186/1471-2164-15-478

Scherer SW, Lee C, Birney E, Altshuler DM, Eichler EE, Carter NP, Hurles ME, Feuk L. 2007. Challenges and standards in integrating surveys of structural variation. *Nat Genet* **39:** S7–S15. doi:10.1038/ng2093

Seburn KL, Nangle LA, Cox GA, Schimmel P, Burgess RW. 2006. An active dominant mutation of glycyl-tRNA synthetase causes neuropathy in a Charcot-Marie-Tooth 2D mouse model. *Neuron* **51:** 715–726. doi:10.1016/j.neuron.2006.08.027

Shaffer LG, Lupski JR. 2000. Molecular mechanisms for constitutional chromosomal rearrangements in humans. *Annu Rev Genet* **34:** 297–329. doi:10.1146/annurev.genet.34.1.297

Sloter E, Nath J, Eskenazi B, Wyrobek AJ. 2004. Effects of male age on the frequencies of germinal and heritable chromosomal abnormalities in humans and rodents. *Fertil Steril* **81:** 925–943. doi:10.1016/j.fertnstert.2003.07.043

Tateno H, Miyake Y-I, Mori H, Kamiguchi Y, Mikamo K. 1994. Sperm chromosome study of two bulls heterozygous for different Robertsonian translocations. *Hereditas* **120:** 7–11. doi:10.1111/j.1601-5223.1994.00007.x

Thorvaldsdóttir H, Robinson JT, Mesirov JP. 2013. Integrative Genomics Viewer (IGV): high-performance genomics data visualization and exploration. *Brief Bioinf* **14:** 178–192. doi:10.1093/bib/bbs017

Vasilevska M, Ivanovska E, Kubelka Sabit K, Sukarova-Angelovska E, Dimeska G. 2013. The incidence and type of chromosomal translocations from prenatal diagnosis of 3800 patients in the republic of Macedonia. *Balkan J Med Genet* **16:** 23–28. doi:10.2478/bjmg-2013-0027

Wang Y, Gao Y, Imsland F, Gu X, Feng C, Liu R, Song C, Tixier-Boichard M, Gourichon D, Li Q, et al. 2012. The crest phenotype in chicken is associated with ectopic expression of *HOXC8* in cranial skin. *PLoS One* **7:** e34012. doi:10.1371/journal.pone.0034012

Wang M, Hancock TP, Chamberlain AJ, Vander Jagt CJ, Pryce JE, Cocks BG, Goddard ME, Hayes BJ. 2018. Putative bovine topological association domains and CTCF binding motifs can reduce the search space for causative regulatory variants of complex traits. *BMC Genom* **19:** 395. doi:10.1186/s12864-018-4800-0

Weckselblatt B, Rudd MK. 2015. Human structural variation: mechanisms of chromosome rearrangements. *Trends Genet* **31:** 587–599. doi:10.1016/j.tig.2015.05.010

Xiang H, Noonan EJ, Wang J, Duan H, Ma L, Michie S, Boxer LM. 2011. The immunoglobulin heavy chain gene 3′ enhancers induce *Bcl2* deregulation and lymphomagenesis in murine B cells. *Leukemia* **25:** 1484–1493. doi:10.1038/leu.2011.115

Yatsenko SA, Rajkovic A. 2019. Genetics of human female infertility. *Biol Reprod* **101:** 549–566. doi:10.1093/biolre/ioz084

Ye L, Morse LR, Zhang L, Sasaki H, Mills JC, Odgren PR, Sibbel G, Stanley JRL, Wong G, Zamarioli A, et al. 2015. Osteopetrorickets due to *Snx10* deficiency in mice results from both failed osteoclast activity and loss of gastric acid-dependent calcium absorption. *PLoS Genet* **11:** e1005057. doi:10.1371/journal.pgen.1005057

Yerle M, Goureau A, Gellin J, Le Tissier P, Moran C. 1994. Rapid mapping of cosmid clones on pig chromosomes by fluorescence in situ hybridization. *Mamm Genome* **5:** 34–37. doi:10.1007/BF00360565

Yu Y, Ouyang Y, Yao W. 2018. shinyCircos: an R/Shiny application for interactive creation of Circos plot. *Bioinformatics* **34:** 1229–1231. doi:10.1093/bioinformatics/btx763

Zhao R, Talenti A, Fang L, Liu S, Liu G, Chue Hong NP, Tenesa A, Hassan M, Prendergast JGD. 2022. The conservation of human functional variants and their effects across livestock species. *Commun Biol* **5:** 1003. doi:10.1038/s42003-022-03961-1

Received February 15, 2023; accepted in revised form May 19, 2023.